

**Impact of heat treatment on mechanical behaviour of Inconel 718 processed with tailored microstructure by selective laser melting**

Popovich, V. A.; Borisov, E.V.; Popovich, A.A.; Sufiiarov, V. Sh; Masaylo, D.V.; Alzina, L.

**DOI**

[10.1016/j.matdes.2017.05.065](https://doi.org/10.1016/j.matdes.2017.05.065)

**Publication date**

2017

**Document Version**

Final published version

**Published in**

Materials & Design

**Citation (APA)**

Popovich, V. A., Borisov, E. V., Popovich, A. A., Sufiiarov, V. S., Masaylo, D. V., & Alzina, L. (2017). Impact of heat treatment on mechanical behaviour of Inconel 718 processed with tailored microstructure by selective laser melting. *Materials & Design*, 131, 12-22. <https://doi.org/10.1016/j.matdes.2017.05.065>

**Important note**

To cite this publication, please use the final published version (if applicable). Please check the document version above.

**Copyright**

Other than for strictly personal use, it is not permitted to download, forward or distribute the text or part of it, without the consent of the author(s) and/or copyright holder(s), unless the work is under an open content license such as Creative Commons.

**Takedown policy**

Please contact us and provide details if you believe this document breaches copyrights. We will remove access to the work immediately and investigate your claim.



# Impact of heat treatment on mechanical behaviour of Inconel 718 processed with tailored microstructure by selective laser melting



V.A. Popovich<sup>a,\*</sup>, E.V. Borisov<sup>b</sup>, A.A. Popovich<sup>b</sup>, V.Sh. Sufiiarov<sup>b</sup>, D.V. Masaylo<sup>b</sup>, L. Alzina<sup>c</sup>

<sup>a</sup> Delft University of Technology, Department of Materials Science and Engineering, Delft, The Netherlands

<sup>b</sup> Peter the Great Saint-Petersburg Polytechnic University, 29, Polytechnicheskaya, 195251 Saint Petersburg, Russia

<sup>c</sup> SIGMA Clermont, Campus des Cézeaux, 63178 Aubiere Cedex, France

## ARTICLE INFO

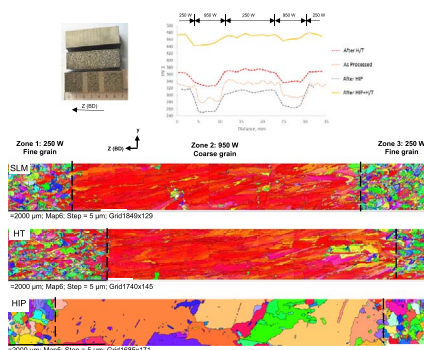
### Keywords:

Additive manufacturing  
Ni-base alloy  
Microstructural design  
Heat treatment  
Mechanical properties

## ABSTRACT

Additive manufacturing (AM) technologies are known to allow the production of parts with an extreme degree of complexity, enabling design and functional part optimization. However, the resulting microstructures and mechanical properties of AM materials are not well understood due to unique and complex thermal cycles observed during processing. This study aims to adjust the microstructure of Inconel 718 specimens produced by selective laser melting (SLM). The microstructural design was achieved through process parameters manipulation and post-process heat treatment. The effects of heat treatment on microstructure, process induced defects, deformation behaviour and failure mechanisms were studied. Directional columnar grained microstructure accompanied by interdendritic Laves phases and carbide particles was observed in as-processed material. Hot isostatic pressing (HIP) improved mechanical properties, which was attributed to dissolution of undesirable Laves and  $\delta$ -phase as well as pore closure. All investigated samples maintained their intended tailored microstructural build up with distinct differences in mechanical properties. The results presented in this study show the capability of the SLM process to produce parts with mechanical properties better than conventional Inconel material. The microstructural design demonstrated here can be exploited in AM fabrication of complex components requiring challenging high-temperature mechanical performance.

## GRAPHICAL ABSTRACT



## 1. Introduction

Nickel-based alloys are widely used in aircraft turbines, jet engines

and steam turbine power plants with service temperatures up to  $\sim 700$  °C, because of their high temperature corrosion, fatigue and creep resistance [1–3]. Inconel 718 is a Ni-based superalloy

\* Corresponding author.

E-mail address: [v.popovich@tudelft.nl](mailto:v.popovich@tudelft.nl) (V.A. Popovich).

strengthened primarily by  $\gamma''$ -Ni<sub>3</sub>Nb and  $\gamma'$ -Ni<sub>3</sub>(Al,Ti) precipitates and which is generally processed by conventional metallurgical routes such as forging (for disks and shafts) and casting (for turbine frames with larger size and more complex geometries) [4–7]. However, owing to the slow cooling rate during solidification, the cast components have coarse grain size, dendritic segregation and solidification defects, leading to poor mechanical properties. Moreover, in a wrought form it is difficult to control the performance of this material and produce complex geometries [8,9].

Selective laser melting (SLM) is an additive manufacturing (AM) process that offers several advantages compared to conventional technologies, like reduction of production steps, high flexibility, low material consumption and, the most importantly, the possibility to manufacture parts with high geometrical complexity and dimensional accuracy. However, due to the complexity of the non-equilibrium SLM process, such problems as residual stresses, porosity, directional grain growth, microsegregation, creation of non-equilibrium phases, and other process induced defects have to be systematically studied. In order to avoid the occurrence of undesirable microstructural features, preserve appropriate precipitate distributions, control the inherent anisotropy and allow further microstructural design, post-processing heat treatment is required.

The majority of the current studies related to SLM using Inconel 718 are concentrated on the macroscopic properties, paying less attention to the microstructure, phase composition and crystallographic texture and its relation to mechanical properties [10,11]. Furthermore, extensive work has been conducted on AM producing single component Ni-based super alloy parts [12–15]; however, little attention has been paid to the study of microstructural design of such components [16,17]. In our previous study [18] it was shown that the grain structure and crystallographic texture of Inconel 718 can be changed during SLM processing by adapting the scanning strategy and the local solidification conditions. Thereby, the capability of additive manufacturing to create tailored microstructure and mechanical properties of the produced part was demonstrated [18].

The scope of this study is to investigate the effect of heat treatment and to verify if the preferred texture and microstructure remain within intended microstructural zones. Furthermore, the impact of post heat treatments, such as homogenisation, aging and hot isostatic pressing on metallurgical mechanisms and mechanical properties has been studied. The results of SLM fabricated parts are further compared with material processed via conventional routes, such as casting and forging.

In the present work the Inconel 718 with tailored microstructure was produced using the SLM technique featuring different laser sources and scanning strategy and resulting in local functionalities via crystallographic texture, grain size and anisotropy optimization. The microstructures of both the X–Y and Y–Z sections have been observed and analysed by scanning electron microscopy (SEM). By applying electron back scattering diffraction (EBSD), the texture and grain morphology were studied to show the anisotropy of the produced microstructural zones. Furthermore, the influence of heat treatment and the columnar grain microstructure on mechanical performance at room and elevated temperature has been examined in detail.

## 2. Experimental

An SLM 280HL system (SLM Solutions Group AG, Germany) featuring two YLR-lasers with a wavelength of 1070 nm and a maximum output power of 400 W and 1000 W was used to produce the materials tested in this study (see Table 1 for process parameters). The laser power, scanning speed and hatch distance were used as variables and optimized in order to produce different parts with the same energy density (Table 1). The layer thicknesses are multiples of each other, meaning that the thicker layer should consist of a number of full thinner layers. Laser power of 250 W and 950 W was used to produce different microstructural areas within blocks of 70 × 20 × 10 mm (Fig. 1), further referred to as samples with 950 W and 250 W zones. Gas atomized Inconel 718 powder (see [18] for chemical composition) was used to fabricate the tested material.

The Z-axis was defined parallel to the building direction, whereas each layer was deposited parallel to the XY-plane with the laser scanning at 45° between X and Y. A “chess-board” scanning strategy with squares of 10 × 10 mm for 250 W and 20 × 20 mm for 950 W was employed in this study. After building up and post treatment, all specimens were machined into their final tensile bar contour by electro-discharge machining (EDM). Residue from EDM was removed by grinding and polishing to 3 μm.

Different post heat treatments were applied to examine the effect on microstructure and mechanical properties of Inconel 718 with tailored microstructure. The samples were investigated under “as-processed”, “heat treated (H/T)”; “hot isostatic pressed (HIP)” and “HIP + H/T” conditions in accordance with AMS 5664E (see Table 2 for heat treatment details). In order to avoid contamination with oxygen, all heat treatments were conducted in argon atmospheres [19].

Vickers hardness profile measurements were performed under 1 kgf (further denoted as HV1). Tensile testing of specimens taken from the YZ plane (see Fig. 1) and ground to 3 μm was carried out with a Zwick 100 kN load cell at a loading rate of 1.5 mm/min. A contact clip gauge (extensometer) with a span of 30 mm was used to record tensile strains. Average tensile properties were calculated based on 5 samples tested per process condition. It should be noted that the values of yield strength (measured as the 0.2% offset) and Young's modulus were calculated from the elastic region data taken from extensometer readings. Ultimate tensile strength and elongation were taken from global measurements. High temperature tensile testing was performed at 650 °C with Zwick/Roell Z100 at a strain rate of 2 mm/min using cylindrical samples (d<sub>0</sub> = 5 mm) according to ISO 6892-2 [20].

Digital image correlation was performed in order to evaluate the strain evolution in the gauge length of tensile samples as a function of applied cross-head displacement (see [21] for further details of the procedure). All images have been correlated using the Istra 4D software package (Limes GmbH) with a facet size of 17 pixels and grid spacing of 7 pixels.

Samples of each of the heat treated conditions taken from YZ planes were prepared for microstructural examination by grinding and polishing down to 1 μm. In order to reveal grain size and morphology, the specimens were etched in Glyceregia reagent (15 ml HCl, 10 ml glycerol and 5 ml HNO<sub>3</sub>) and to reveal precipitates in Kalling's reagent (40 ml HCl, 2 g CuCl<sub>2</sub> and 40 ml ethanol). Optical microscopy was carried out on a Keyence VHX-5000 for microstructure and porosity investigation. A JEOL JSM 6500F scanning electron microscope (SEM) with energy-dispersive spectroscopy was used for microstructural and fracture surface analysis.

X-ray diffraction (XRD) patterns were obtained using Bruker D8 diffractometer with CoK<sub>α</sub> radiation (λ = 1.79020 Å). Diffraction patterns were recorded within the 2θ range from 10° to 110° with a step size of 0.034°. The X-ray beam was collimated to a spot size of 3 mm in diameter on the sample surface.

For electron backscatter diffraction (EBSD) texture characterization, specimens featuring regions processed with a higher laser energy of

**Table 1**  
Process parameters applied for SLM fabrication of specimens.

Laser power (W)	Laser scanning speed (mm/s)	Hatch distance (mm)	Layer thickness (μm)	Volume energy density (J/mm <sup>3</sup> )
250	700	0.12	50	59.5
950	320	0.5	100	59.4

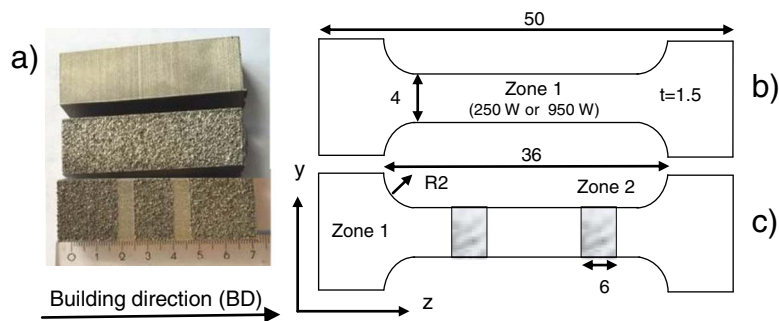


**Fig. 1.** Schematic showing SLM fabricated functional Inconel 718 using a variation of 250 W and 950 W laser sources; a) samples processed in the current study; b) tensile sample geometry used to test the matrix (zone 1) material, processed with 950 W or 250 W; c) geometry with two evenly distributed lines (zone 2) processed with 250 W or 950 W (dimensions are in mm).

**Table 2**

Heat treatment parameters used for post-processing of SLM Inconel 718 [19].

Designation	Heat treatment	Details
H/T	Annealing heat treatment	850 °C/2 h/air cooling (AC)
HIP	Hot isostatic pressing	1180 °C/3 h at 150 MPa pressure. Furnace cooling (FC)
HIP + H/T	Hot isostatic pressing + homogenization + aging	HIPed + 1065 °C/1 h/AC + 760 °C/10 h/FC at 55 °C/h to 650 °C/8 h/AC

950 W embedded in a region (matrix) processed with a lower laser energy of 250 W were ultra-polished with colloidal silica (0.05  $\mu\text{m}$ ). The EBSD analysis was performed using SEM Mira 3 Tescan at accelerating voltage of 20 kV with a step size of 5  $\mu\text{m}$  using Channel 5-HKL software. A total of 14 individual maps (700  $\times$  700  $\mu\text{m}$ ) were stitched together to cover the entire area of interest. EBSD orientation maps were always presented with respect to building direction (Z).

### 3. Results and discussion

#### 3.1. As-processed microstructure

The as-processed microstructure of the Inconel 718 samples viewed in YZ plane depicts the columnar coarse grained architecture for 950 W (Fig. 2b) and a much finer grained microstructure for 250 W (Fig. 2a). The resulted microstructures are similar to directionally solidified components and the direction of the grain growth is determined by the heat flux. As can be seen, section cuts parallel to the building direction show arch-shaped lines, which indicate the melt pool morphology and the cross section of the laser beam scanning paths. The observed significant differences in microstructures (Fig. 2a and b) were used to develop functional materials by modulating the laser scan strategy and process parameters (Fig. 2c). It should be noted, that produced material exhibit a small transition area between the zone, resulting from remelting of the previous layers. The concept and resulting properties of

such specimens with tailored microstructure are presented in our previous publication [18].

Apart from grain morphology, the difference in the thermal conditions of Inconel 718 components affects the residual stress level, grain size and phase composition in the as-processed condition. As can be deduced from the isothermic sections of the Ni–Nb–C equilibrium diagram [22], NbC and Laves-phase particles can be created in the interdendritic spaces as products of eutectic reactions when the concentration of Nb, Mo and C in the melt is sufficiently high. Laves is a brittle, intermetallic phase that forms in Inconel 718 usually as a result of segregation and is considered undesirable [23,24]. Due to the large amounts of Nb required for the phase, Laves usually forms in heavily segregated regions. It is known, that Laves can reduce the mechanical properties of Inconel 718 through several mechanisms with the most dominant probably being brittle fracture of the phase, that provides the conditions for nucleation and crack growth, which severely impairs the plasticity of Inconel 718 at room temperature [25]. In the current work, the formation of Laves and MC-type carbides was observed between aligned dendritic cells and in the region of an overlapping interface between two adjacent laser scanning tracks or layers (Fig. 3). Irregularly shaped Laves phases ( $\sim$ 1–2  $\mu\text{m}$ ) were found to be rich in Nb and Mo and are believed to be a result of Nb segregation in interdendritic regions during the solidification process. Furthermore, Laves phase was primarily found in regions processed with the higher energy laser source, which can be explained by segregation effects during solidification. As previously reported [26], the formation of Laves phase was found to be facilitated by increasing the heat input or lowering the cooling rate. The presence of spherically shaped carbides, found in this study, indicate their primary formation in liquid before the Laves reaction. EDS analysis showed that the carbides are rich in Nb and Ti.

Hence, in order to avoid the occurrence of such undesired microstructural features, post-processing heat treatment is required.

#### 3.2. Effect of heat treatment on microstructure

In metal additive manufacturing, the standard practice is to use

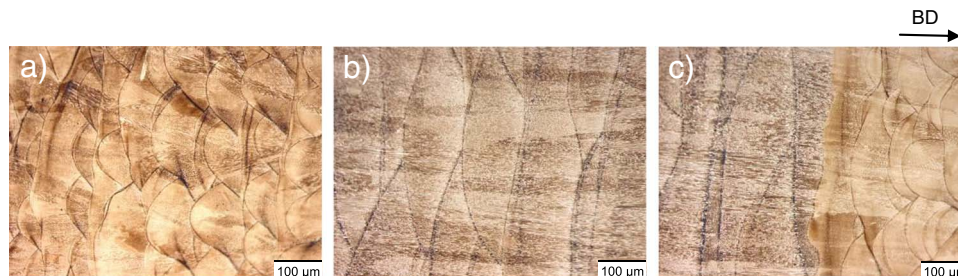


**Fig. 2.** Optical micrographs of as-processed Inconel 718 specimens depicting YZ plane of parts processed with a) 250 W and b) 950 W laser source; c) the boundary between the two zones.

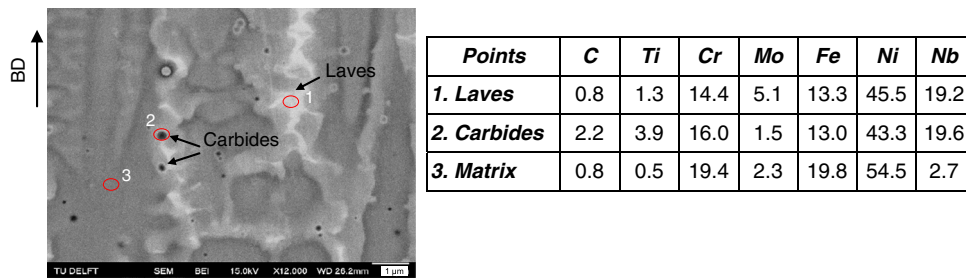


Fig. 3. Back-scattered electron (BSE) image of the coarse grained region (built with 950 W) and an energy dispersive spectroscopy (EDS) analysis showing submicron carbide precipitation.

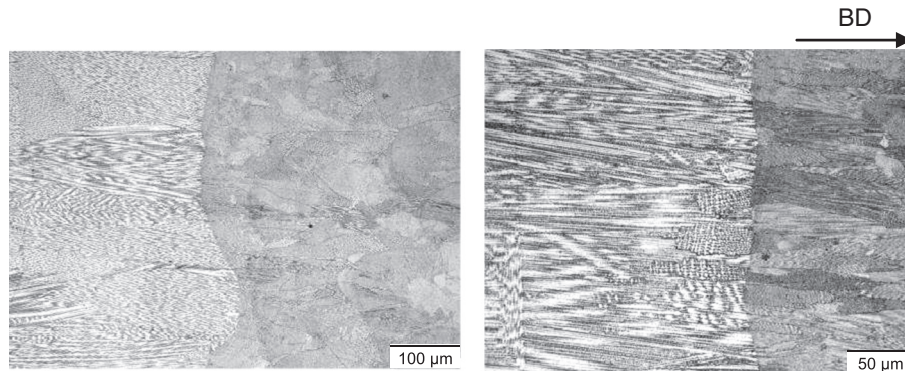


Fig. 4. Optical micrographs of heat treated at 850 °C material showing the transition between zones (950 W zone embedded in 250 W matrix).

some combination of thermal post-processing steps: stress relief, hot-isostatic pressing and aging before the final in-service application [27,28]. These steps are designed to relieve stress, reduce porosity and produce a desired precipitate distribution in the microstructure. In this work, three post-processing conditions, including heat treatment at 850 °C, HIP and HIP + homogenization + aging (HIP + H/T) were used and their effects on microstructure and mechanical properties were evaluated separately.

As can be seen from Fig. 4, the microstructure after heat treatment maintained its columnar nature and traces of layered build up, which indicates that recrystallization did not take place. However, residual particles of the Laves phase and a large amount of the needle-like  $Ni_3Nb$ - $\delta$  precipitates (with solvus temperature of  $\sim 1010$  °C [28]) are observed on grain and sub-grain boundaries and along the layer interfaces (Fig. 5).

Replacement of Laves phase within the interdendritic areas by a network of small 500 nm long delta phase needles is most likely

associated with the niobium present from the dissolution of the Laves phase [28]. It should be noted, that the extra precipitated phases are strengthening  $\gamma''$ - and  $\gamma'$ -phases, which precipitate between 600 °C and 900 °C and form a basis for the precipitation hardening of this alloy. These phases have distinctly different morphologies, which help in their identification;  $\gamma'$ -phases ( $Ni_3(Al,Ti)$ ) are round shaped and about 20 nm in size, while  $\gamma''$ -precipitates ( $Ni_3Nb$ ) are disk-like with an aspect ratio of 5–6 (Fig. 5) [23]. However, as it has been previously observed [23–25], at temperatures higher than 650 °C, the  $\gamma''$ -phase is unstable and will transform into the more stable  $\delta$ -phase. While  $\delta$ -phase precipitates have the same composition as  $\gamma''$ -phase precipitates (bcc structure  $Ni_3Nb$ ),  $\delta$ -phase precipitates have an orthorhombic crystal structure and are incoherent with the austenite matrix. Accordingly, the strengthening effect of  $\delta$ -phase precipitates on the matrix is generally considered to be negligible.

The  $Ni_3Nb$   $\delta$ -phase cannot be precipitated during the SLM process due to the high cooling rate and small content of Nb caused by the

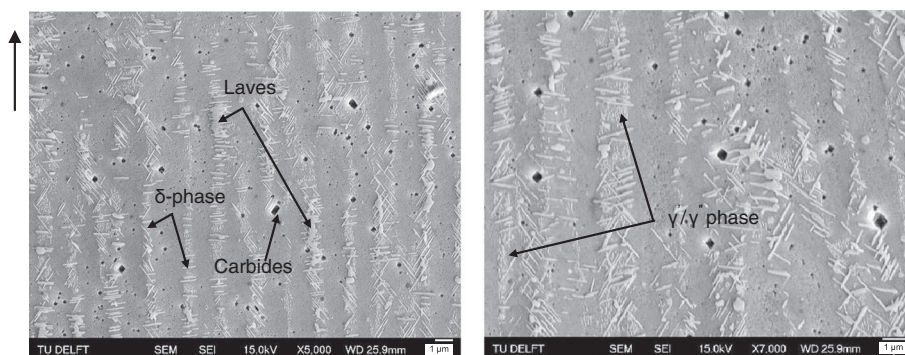


Fig. 5. SEM images of as-heat treated microstructure of 950 W zone, depicting precipitates.

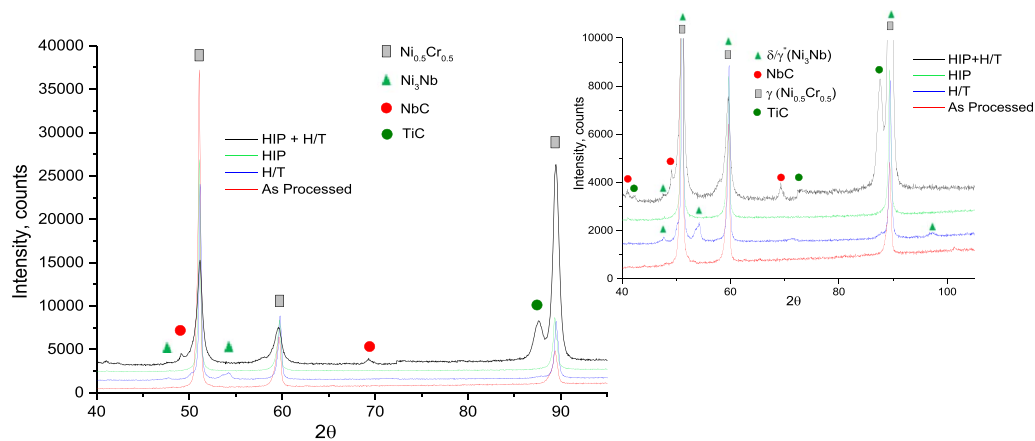


Fig. 6. XRD patterns (including enlarged insert from the main graph) showing as-processed, heat treated (H/T), hot isostatic pressed (HIP) and HIP + H/T areas of Inconel 718 produced via SLM with 950 W laser source.

occurrence of abundant Laves phase. However, as can be seen, the precipitation of  $\delta$ -phase occurs following heat treatment for 2 h at 850 °C, which is further confirmed by the strong peaks of  $\text{Ni}_3\text{Nb}$  found by XRD (Fig. 6). It is, however, difficult to quantify and differentiate between  $\gamma''$ -phase ( $\text{Ni}_3\text{Nb}$ ) and  $\delta$ -phase, as both have coinciding peaks.

Another post-process applied in this study is hot isostatic pressing (HIP). The HIP process is usually used to close pores and flaws by plastic flow, which results in improved strength, ductility and fatigue life of materials with significantly less variation from lot to lot [29].

In all as-HIPed samples studied herein, there is a significant pore closure (see porosity results presented in the next section, Table 3) and grain growth observed. Moreover, as can be seen from Fig. 7, the HIP process did not remove the columnar grain architecture and a clear transition between the fine and coarse grained zones is preserved.

SEM images (Fig. 8) of as-HIPed samples show preferred NbC precipitate network ordered in columns along dendrite boundaries parallel to the building direction. The presence of NbC was further confirmed by XRD (Fig. 6).

The lump carbides ( $\sim 1 \mu\text{m}$ ) appear at the grain-boundaries, contrary to unevenly distributed carbides observed in the heat treated condition (Fig. 5), which is beneficial for the strength of the material, as these carbides can prevent the grain boundaries sliding [32]. No Laves

phase was detected in the as-HIPed condition, which indicates that the applied temperature was sufficiently high for its dissolution. Hence, it is evident that microstructure homogenization and dissolution of metastable phases took place as a result of HIP process (Figs. 7 and 8).

The HIPed + H/T samples, shown in Fig. 9, keep their intended tailored microstructure with distinct transition between fine and coarse grained areas. A similar grain size was observed in the HIPed samples before and after heat treatment, which is attributed to the presence of prior boundary particles decorated with NbC (Fig. 10), impeding the grain growth. Furthermore, small TiC particles ( $\sim 200 \text{ nm}$ ) were observed evenly distributed throughout the matrix and when compared with as-HIPed condition, the carbide population appears increased after the heat treatment. In addition to the higher carbide density, needle-like  $\delta$ -phase was detected along the grain boundaries (see Fig. 10). The formation of  $\delta$ -phase with a platelet morphology can occur in Inconel alloys in the temperature range between 650 and 980 °C [30]. It has previously been observed [29,31], that the  $\delta$ -phase platelets grow into the surrounding grains, leading to inferior strength and restricting grain growth.

Table 3

A summary of tensile properties at room temperature, hardness and porosity of monolithic and tailored specimens produced with different laser powers (performed on flat samples).

Samples name and laser source	Yield strength 0.2%, (MPa)	Young's modulus (GPa)	Elongation to failure (%)	Tensile strength (MPa)	Hardness, 250 W/950 W HV <sub>1</sub> kgf	Porosity 250 W/950 W%
Monolithic, not tailored material						
As-processed						
Cast [32]	488	200	11	752	353	–
Wrought [24]	916	200	17	1055	353	–
SLM - 250 W	668 ± 16	173 ± 13	22 ± 2	1011 ± 27	320	0.11
SLM - 950 W	531 ± 9	113 ± 3	21 ± 5	866 ± 33	287	0.27
SLM + Heat treatment						
250 W	875 ± 11	190 ± 11	17 ± 2	1153 ± 4	360	0.15
950 W	668 ± 7	138 ± 5	7 ± 2	884 ± 80	338	0.29
SLM + hot isostatic pressing						
250 W	645 ± 6	188 ± 8	38 ± 1	1025 ± 14	310	0.02
950 W	481 ± 11	183 ± 19	34 ± 3	788 ± 12	262	0.06
SLM + hot isostatic pressing + heat treatment						
250 W	1145 ± 16	190 ± 6	19 ± 1	1376 ± 14	468	0.04
950 W	1065 ± 20	188 ± 20	15 ± 4	1272 ± 12	451	0.07
Tailored SLM material: zone 1–250 W Matrix and zone 2 - two lines of 950 W						
As-processed	574 ± 6	136 ± 13	13 ± 2	873 ± 14	330	0.09
After H/T	704 ± 8	167 ± 13	4 ± 2	920 ± 53	370	0.06
After HIP	500 ± 6	187 ± 8	21 ± 1	817 ± 16	310	0.04
HIP + H/T	1041 ± 47	196 ± 15	7 ± 1	1154 ± 68	478	0.05

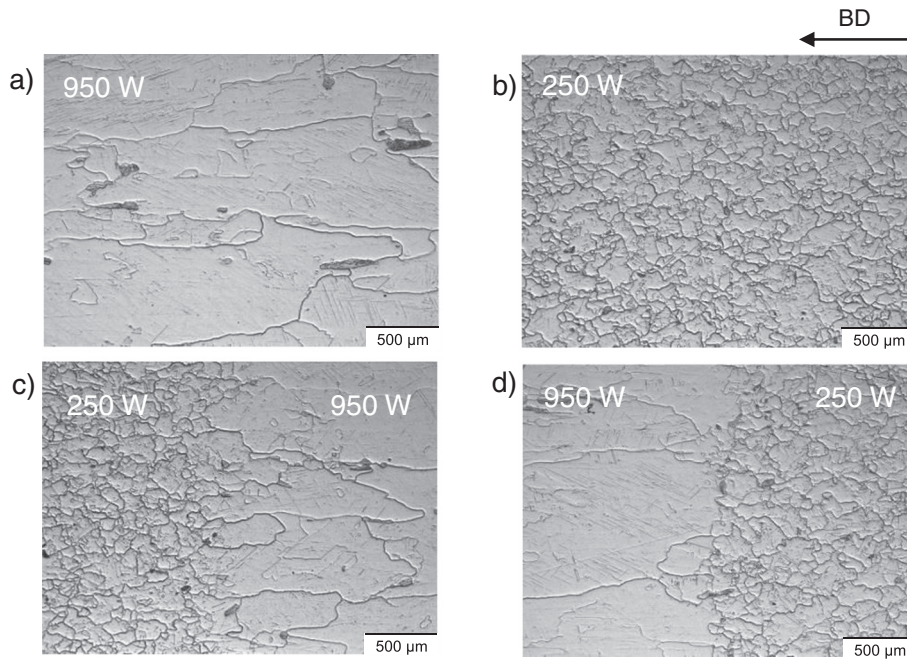


Fig. 7. Optical micrographs of the material after hot isostatic pressing showing transition between the zones (950 W zone embedded in 250 W matrix).

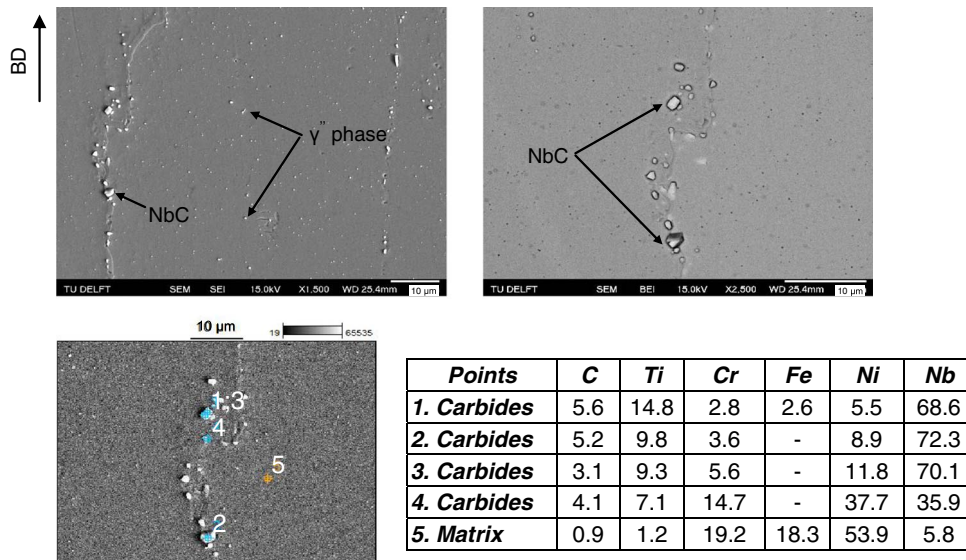


Fig. 8. SEM images of hot isostatically pressed (HIP) samples, processed with 950 W.

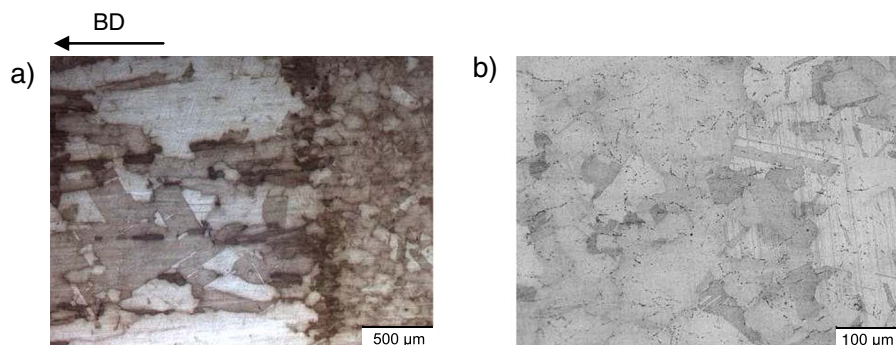


Fig. 9. Optical images of Inconel 718 after HIP + H/T a) transition area between 250 W and 950 W zones, revealed via Glyceregria reagent b) area depicting the presence of precipitations and twins, revealed via Kalling's reagent.

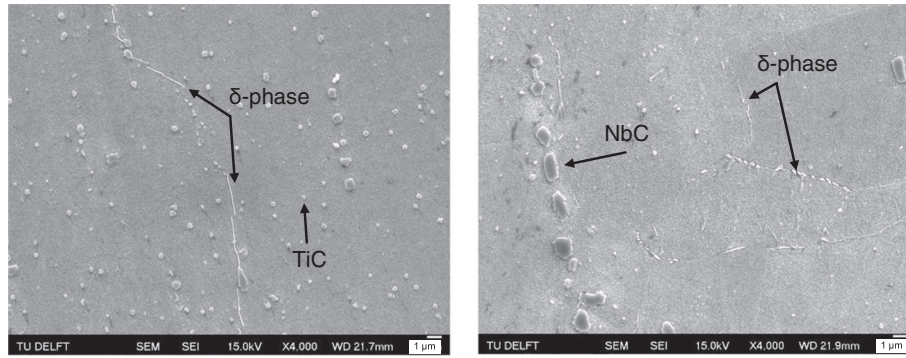


Fig. 10. SEM images of 950 W HIPed + H/T samples, depicting carbides and precipitates.

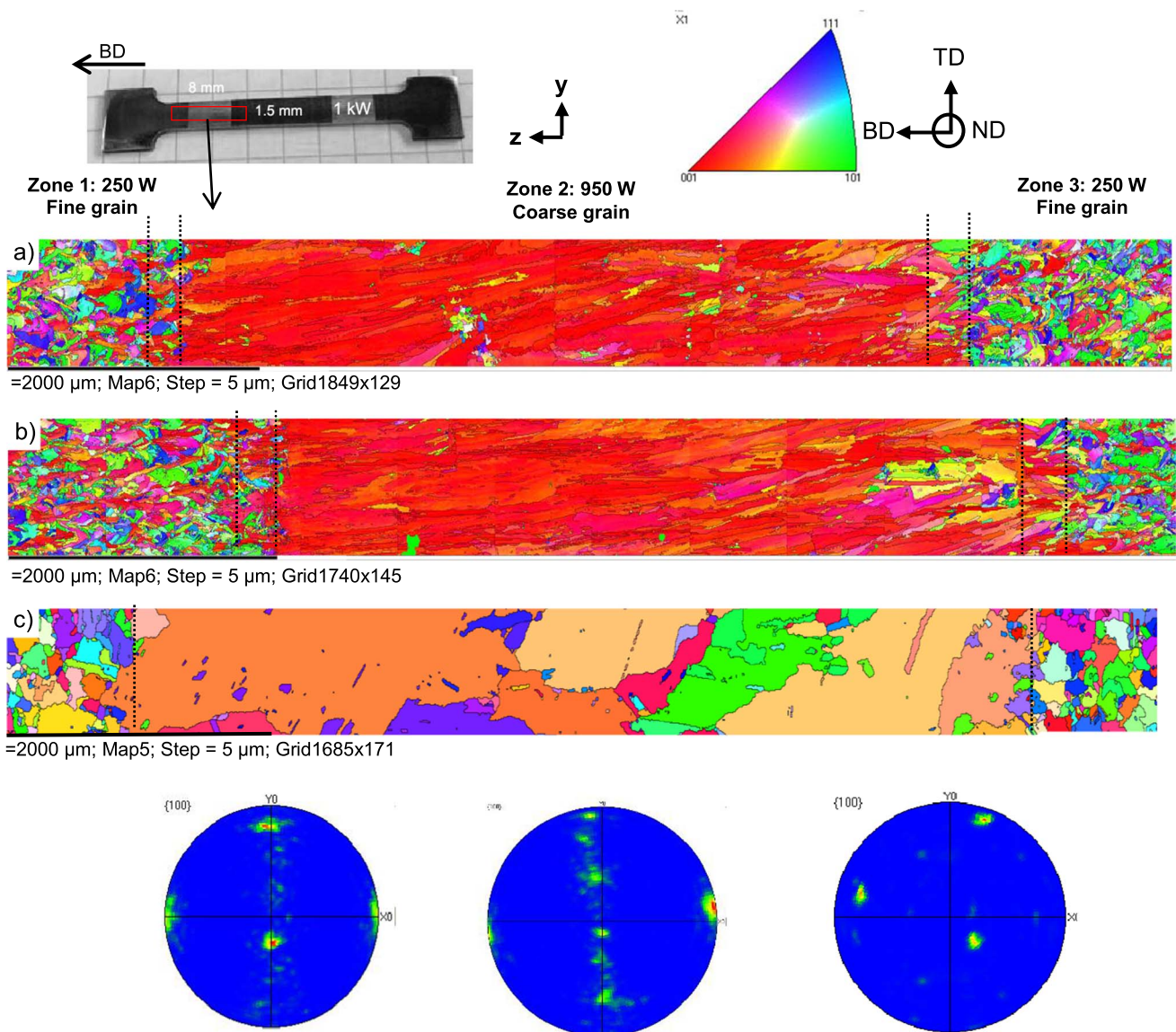


Fig. 11. EBSD analysis of an Inconel 718 sample featuring a single coarse columnar grained zone embedded in a fine grained matrix (black dotted lines indicate transition areas between the zones) a) Inverse Pole Figure (IPF) coloured map of as-processed Y-Z section b) IPF of as-heat treated c) IPF after HIP and Pole figures of the texture for zone 2 for d) as-processed e) as-heat treated f) after hot isostatic pressing (HIP). (For interpretation of the references to colour in this figure, the reader is referred to the web version of this article.)

### 3.3. Effect of heat treatment on crystallographic texture

EBSD analysis (Fig. 11) was performed to provide a deeper look into the crystallographic texture of the processed specimens and verify the

effect of heat treatment. It should be noted that in the current study the z-axis is parallel to the building direction, whereas the x-y plane is the building platform plane. As can be seen from Fig. 11a and b, there is a clear and sharp transition between the coarse and fine grained areas for

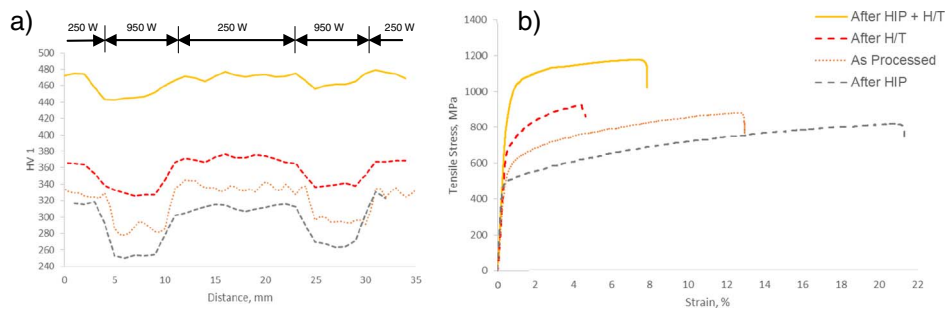


Fig. 12. Effect of heat treatment on a) hardness profile and b) tensile properties of specimens with tailored microstructure featuring two zones produced with 950 W.

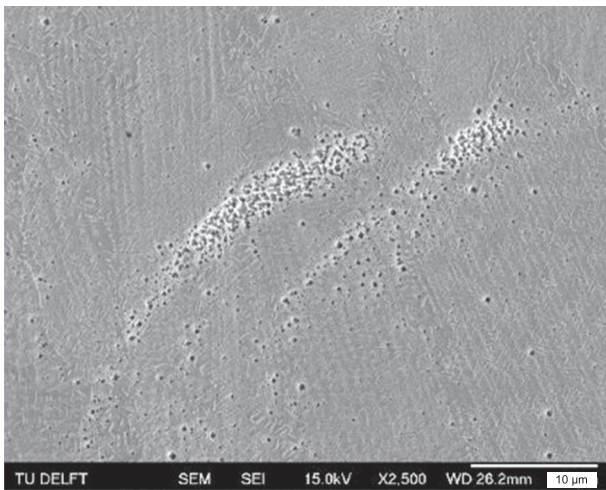


Fig. 13. SEM image of the heat treated 250 W zone showing persistence of solidification porosity and carbide “holes”, where small carbides have been removed as a result of sample preparation.

the as-processed and heat treated conditions. Furthermore, the columnar grained region has elongated grains with a (001) orientation with respect to building direction, i.e. the direction of predominant heat flux during processing (as depicted by the red colour, Fig. 11a and b). Both conditions seem to have a strong {100} texture (Fig. 11d, e), with the fine grained zone showing equiaxed grain structure and a rather chaotic orientation. The results obtained indicate that heat treatment does not cause recrystallization.

However, it was found that during HIP processing at 1180 °C recrystallization starts and leads to the formation of different microstructures (see Figs. 7 and 8). As can be deduced from Fig. 11c, grain coarsening and a change in crystallographic texture occurs after HIP

Table 4

Tensile properties of Inconel 718 at 650 °C (performed on cylindrical samples).

Samples name and laser source	Yield strength 0.2%, (MPa)	Elongation to failure (%)	Tensile strength (MPa)
Cast [34]	517	13	576
Wrought [34]	955	14	1061
As-processed			
SLM - 250 W	650 ± 11	28 ± 4	845 ± 9
SLM - 950 W	543 ± 2	31 ± 6	782 ± 6
SLM + hot isostatic pressing			
250 W	626 ± 8	29 ± 1	857 ± 14
950 W	479 ± 5	28 ± 2	665 ± 7
SLM + hot isostatic pressing + heat treatment			
250 W	942 ± 11	20 ± 2	1078 ± 8
950 W	872 ± 13	17 ± 4	1005 ± 12

processing. Nonetheless, it should be noted, that the majority of coarse grains in the 950 W zone seem to keep their preferred (001) orientation and there is still a clear transition between the coarse and fine grained areas. HIP + H/T condition did not change crystallographic texture and EBSD analysis revealed similar to HIP microstructure. Hence, it appears that the local deformation during HIP processing and the high temperatures provide driving forces large enough to promote recrystallization, but not enough to erase tailored microstructure build up.

### 3.4. Effect of heat treatment on mechanical properties

As can be seen from Fig. 12, there is a steep gradient in hardness between created microstructural zones and it is evident that a stacking sequence of coarser and finer grained regions has an influence on local

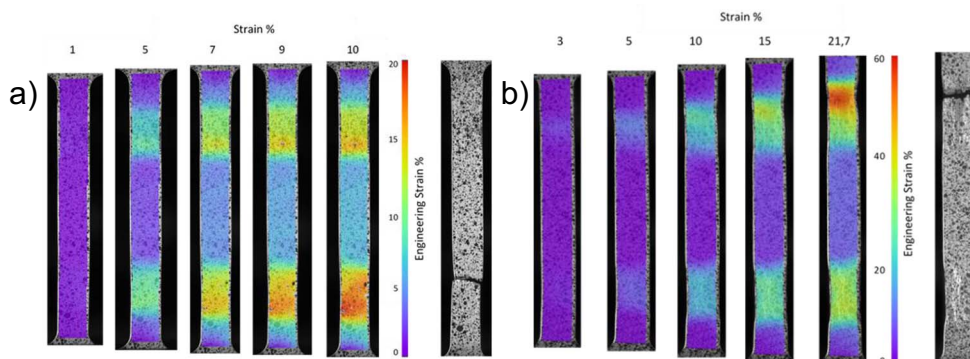


Fig. 14. DIC showing strain evolution as a function of cross head displacement (shown for specimens with two coarse grained regions) for a) as-processed and b) after HIP process.

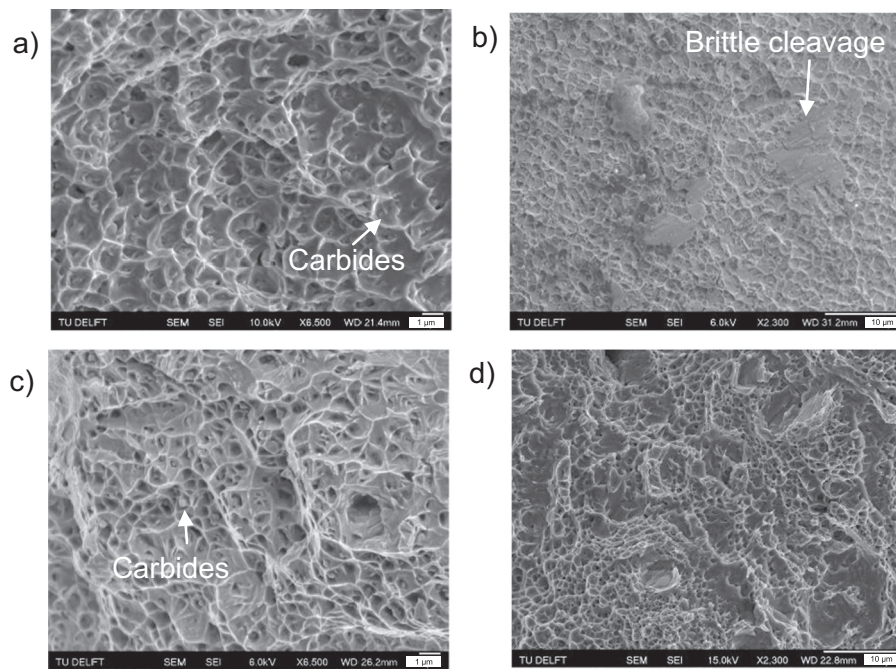


Fig. 15. Fracture surfaces of a) As-processed b) After H/T c) after HIP d) HIP + H/T tailored specimens broken in 950 W area.

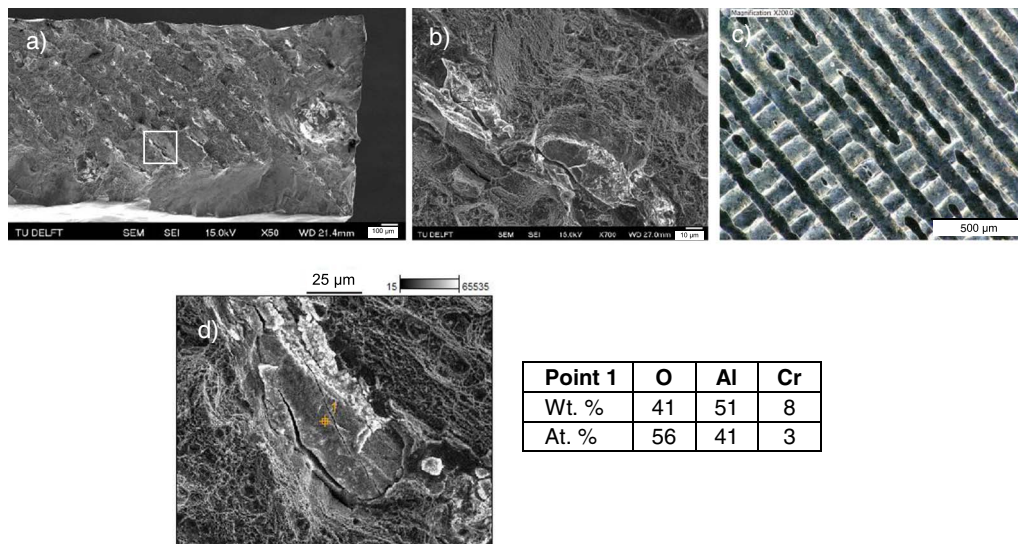


Fig. 16. Fracture surface (a and b) of HIP + H/T samples, showing repetitive fracture lines (magnified region is outlined); c) top view of the sample, depicting scanning path (strategy) in a form of overlapping at 45° layers d) EDS spot analysis of the enlarged cracked area revealing the presence of oxide phase. Building direction is perpendicular to the image plane.

mechanical properties. Furthermore, post-process heat treatment has a significant effect on mechanical properties (Fig. 12a and b). An increase of hardness by 10% for the as-heat treated condition is most likely attributable to precipitation hardening by  $\delta$ -phase (see Fig. 5), which acts as a barrier for dislocation motion, thus improving hardness.

Contrary to the heat treated condition, a hardness decrease by 10% for HIP processed samples is attributed to microstructure homogenization and dissolution of metastable phases, as seen in Figs. 7 and 8. An addition of a heat treatment to the HIP condition results in a smoother gradient and a substantial hardness increase up to 480 HV, which is due to the increased carbide size and density as well as precipitation of the  $\delta$ -phase (Figs. 10 and 12).

An overview of room temperature mechanical properties for all examined materials is presented in Table 3. The tensile properties

including yield strength, tensile strength, elongation to failure, Young's modulus and hardness are presented for monolithic and tailored materials and compared with conventional cast and wrought Inconel 718.

As can be seen, the tensile properties of the SLM deposited material are superior to the cast samples for both laser processing conditions. However, the properties are inferior to the wrought material properties, with the exception to the elongation, that is better for the SLM produced samples. There is a reduction of tensile and yield strength by 20% for the 950 W matrix compared to the 250 W matrix. Furthermore, elongation fluctuations for 950 W are most likely attributable to localized porosities in the build samples, as solidification shrinkage porosity was present [18]. The overall reduction in tensile properties for 950 W is a result of coarse grains preferably oriented in the (001) direction. Hence, the observed mechanical properties are primarily dependant on

the grain size and texture. However, it is expected that coarse grains elongated along the (001) direction will be beneficial for high temperature properties, such as thermomechanical fatigue and creep [27].

Fig. 12b shows a comparison of corresponding stress-strain curves for tailored as-processed, heat treated, HIP and HIP + H/T Inconel material. It should be mentioned that for all studied post treatment conditions there is a remarkable correlation between strength and hardness, which confirms the need of finding the most appropriate (for the desired application) trade-off between strength, ductility and hardness. As seen, post heat treatment improves the tensile strength and hardness, which is attributed to the presence of the  $\delta$ -phase at the grain boundaries. The reason for that is the presence of thin and long needles (Fig. 5), which provide restrictions to the grain boundary movement such as sliding [32]. Hence, grain boundary phases precipitated by heat treatment act as a barrier for dislocation motion, thus improving the strength of SLM built material. Conversely, a significant reduction in elongation to failure, can be explained by the presence of large carbides, Laves phase and porosity. As can be seen from Figs. 5 and 13, there is a clear evidence of cuboidal shaped Nb-rich and/or Ti-rich MC primary carbides unevenly distributed throughout the material. It should be noted, that carbides in as-heat treated samples are coarsened ( $\sim 1 \mu\text{m}$ ) as compared to the as-built condition (carbides ranging from 100 nm to 200 nm).

After hot isostatic pressing, the dominating effect of pores and subphases disappeared and the strength became more dominated by the grain size as dictated by the Hall-Petch relation [33]. Furthermore, the lower strength and improved elongation as compared to as-processed condition can be related to Laves phase dissolution, NbC precipitation and reduction of porosity. Hence, fracture behaviour of this material is primarily determined by the monotonic strength and not the process-induced defects such as pores. Upon further heat treatment of as-HIPed material the yield strength increases by a factor of two, however the elongation drops back to the level of as-processed condition. Moreover, the application of HIP + H/T post treatment results in superior to cast and wrought mechanical properties (Table 3). Furthermore, HIP and HIP + HT samples exhibit homogeneous distribution of spherical  $\sim 1\text{--}3 \mu\text{m}$  pores, which might be beneficial for fatigue lifetime.

Digital image correlation (DIC) of specimens with tailored microstructure was performed in order to study room temperature local strain distribution as a function of post-process heat treatment. The strain patterns for the tailored as-processed and as-HIPed material featuring two coarse grained zones is shown in Fig. 14. The strain evolution was similar for all tested specimens, with coarse grained regions featuring highest deformation and a final failure point. The results presented show a clear evidence that HIP post treatment did not remove intended microstructural differences and material retains its locally created mechanical properties. The steepness of the strain gradient shown in Fig. 14 is in good agreement with the hardness profile presented in Fig. 12. It should be noted, that even though the as-processed sample broke at 11% of global cross head displacement, the local peak strains in the coarse grained area reached 22.3%, leading to a final failure of the samples in the lower 950 W part (Fig. 14a). The application of HIP process clearly extends the limit of local strain a material can withstand before failure, reaching up to 60%, Fig. 14b.

High temperature tensile properties for monolithic cylindrical samples are summarized in Table 4. The tests were performed at 650 °C and the results are shown as a function of heat treatment. As can be seen, elevated temperature tensile and yield strength of the as-processed samples are inferior to those of the typical wrought Inconel 718 alloy, though their ductility is much higher. After hot isostatic pressing, the tensile strength and ductility are comparative with those of the cast material. However, an application of HIP + H/T results in superior ductility as compared to wrought Inconel 718. Therefore, the tensile properties of the SLM + HIP + H/T material are excellent enough to meet the needs of such high temperature applications, as turbine blades and power plants.

### 3.5. Fracture surface analysis

The fractographic analysis of broken tensile samples was performed in order to understand the effect heat treatment conditions on fracture mechanism and to interpret the tensile properties of the specimens. All tensile samples tested exhibit mostly dimpled surfaces (Fig. 15), which indicates a transgranular ductile failure mode [35]. The as-processed and HIP conditions show a presence of carbides particles, serving as void initiators (Fig. 15 a, c, as indicated by an arrow). Conversely, heat treated samples (Fig. 15b, as indicated by an arrow) exhibit signs of brittle cleavage failure and shallower “flat” voids, which correlate well with low ductility results (see Table 3). The location of brittle fracture corresponds to areas enriched with Nb and matches well the Laves phases observed in Fig. 5. Hence, it is believed, that undissolved Laves phases, present in H/T samples, serve as crack initiation points during tensile testing and consequently reduce the strength. These observations are in good agreement with tensile strength results presented in Table 3.

The fracture surface of HIP + H/T samples appears finely dimpled at large magnifications (Fig. 15d), which corresponds well with the high strength of these samples. However, an analysis at lower magnifications revealed a very distinctive and repetitive fracture pattern, as shown in Fig. 16a. Parallel lines diagonally distributed at 45° and separated by  $\sim 200 \mu\text{m}$  can be clearly seen as cracked brighter areas, appearing on the fractured HIP + H/T samples. EDS spot analysis of the enlarged cracked areas (Fig. 16b) exhibited intensive peaks for Al, O and Cr (Fig. 16d). The chemistry of these brittle areas corresponds well to the composition of  $\text{Al}_2\text{O}_3$ , i.e. 60 at.% O and 40 at.% Al, and indicates that this oxide is sufficiently thick to permit accurate chemical compositional analysis via EDS. The presence of oxide phases has been also observed [36] in direct laser deposited samples processed in inert (argon) atmosphere, which indicates that oxidation of some alloying elements in Inconel 718 cannot be completely avoided during AM manufacturing [36–38].

The exposed surface of the oxide phase, visible from Fig. 16b and d, seems to have poor wetting with the metal, contributing to a lack of bonding or a cracking with the metal. A combination of high surface roughness with non-wetting oxides present in higher energy (950 W) areas may result in a partially melted successive layer, which would explain the 45° lines, corresponding well to the scanning pattern selected for this study (Fig. 16c). It should be noted, that tensile strength was not affected by the presence of oxides and as HIP + H/T samples exhibit strength values superior to wrought Inconel 718. Nevertheless, a suitable control of process conditions and avoidance of oxides is needed in order to further improve the samples ductility.

## 4. Conclusions

The article presents a study related to changes in microstructure and mechanical properties of Inconel 718 alloy with tailored microstructure processed by SLM after different heat treatments. High and low power laser sources were used to process specimens featuring fine and coarse grained areas. The grain structure and precipitates were characterized via SEM-BSE, EDS, EBSD and XRD. Mechanical characterization was conducted by hardness measurements, room and high temperature tensile testing and digital image correlations. The main findings can be summarized below:

1. The as-processed microstructure features distinctive coarse and fine grained zones. Areas processed with higher power show a strongly textured microstructure with long grains elongated in (001) direction. Furthermore, interdendritic Laves phases and carbide particles were observed in as-processed material.
2. Heat treatment did not lead to recrystallization and the desired texture and grain morphology were preserved. A significant

decrease in elongation for as-heat treated condition could be a result of a large amount of the needle-like  $\text{Ni}_3\text{Nb}-\delta$  precipitates and brittle fracture of undissolved Laves phases. Conversely, grain boundary phases precipitated by heat treatment act as a barrier for dislocation motion, thus improving yield strength.

3. Hot isostatic pressing, to the surprise of the authors, retained the sharp microstructural border between fine and coarse grained regions. Furthermore, crystallographic texture in the higher energy processed zones seem to mostly retain its preferred  $\{100\}$  texture.
4. All samples showed significant improvement in mechanical properties after hot isostatic pressing (HIP), which is most likely attributed to dissolution of undesirable Laves and  $\delta$ -phase as well as pore closure. Hence, the dominating effect of defects and subphases disappeared and yield strength became more dominated by the grain size as dictated by the Hall-Petch relation.
5. An addition of H/T step after HIP process resulted in substantial improvement in mechanical properties, which is attributed to the increase in size and density of carbides. Furthermore, the samples retained their intended tailored microstructure. The similar grain size was observed in the HIPed samples before and after heat treatment, which is attributed to the presence of prior boundary particles decorated with NbC carbides, impeding the grain growth.
6. Room temperature tensile properties and high temperature ductility of HIP + H/T samples are superior to those of wrought Inconel 718. However, in spite of using high-purity inert gas protection, oxide phase is observed in SLM Inconel 718 alloy, which results in reduced ductility.

The results presented in this study show the feasibility of producing material with tailored microstructure via SLM processing. By applying HIP + H/T post-processing the intended microstructural build up remained and the resulting mechanical properties became superior to those of cast and wrought Inconel 718.

Thermo-mechanical fatigue and high temperature creep should be investigated in order to fully explore the benefits of microstructural design in SLM Inconel 718. Furthermore, optimization of process parameters should be explored in more details in order to produce a smoother transition between the tailored microstructural regions.

## References

- [1] S. Ghosh, S. Yadav, G. Das, Study of standard heat treatment on mechanical properties of Inconel 718 using ball indentation technique, *Mater. Lett.* 62 (2008) 2619–2622.
- [2] A. Niang, B. Viguiere, J. Lacaze, Some features of anisothermal solid-state transformations in alloy 718, *Mater. Charact.* 61 (2010) 525–534.
- [3] A. Chamanfar, L. Sarrat, M. Jahazi, M. Asadi, A. Weck, A.K. Koul, Microstructural characteristics of forged and heat treated Inconel 718 disks, *Mater. Des.* 52 (2013) 791–800.
- [4] T.S. Chester, S.S. Norman, C.H. William, *Super-alloys II*, John Wiley & Sons, Inc., New York, 1976.
- [5] P. Caron, T. Khan, Evolution of Ni-based superalloys for single Crystal gas turbine blade applications, *Aerosp. Sci. Technol.* 3 (8) (1999) 513–523.
- [6] J. Warren, D.Y. Wei, The cyclic fatigue behavior of direct age 718 at 149, 315, 454 and 538 °C, *Mater. Sci. Eng. A* 428 (2006) 106–115.
- [7] H.Y. Zhang, S.H. Zhang, M. Cheng, Z.X. Li, Deformation characteristics of  $\delta$  phase in the delta-processed Inconel 718 alloy, *Mater. Charact.* 61 (2010) 49–53.
- [8] X. Wang, X. Gong, K. Chou, Review on powder-bed laser additive manufacturing of Inconel 718 parts, *Proc. ASME 2015 International Manufacturing Science and Engineering Conference*, Am. Soc. Mech. Eng. (2015) p. V001T001A002.
- [9] V.Sh. Sufiiarov, A.A. Popovich, E.V. Borisov, I.A. Polozov, Selective laser melting of heat-resistant Ni-based alloy, *Non-Ferrous Met.* 1 (38) (2015) 32–35.
- [10] K. Amato, S. Gaytan, L. Murr, E. Martinez, P. Shindo, J. Hernandez, S. Collins, F. Medina, Microstructure and mechanical behavior of Inconel 718 fabricated by selective laser melting, *Acta Mater.* 60 (5) (2012) 2229–2239.
- [11] Z. Wang, K. Guan, M. Gao, X. Li, X. Chen, X. Zheng, The microstructure and mechanical properties of deposited-IN718 by selective laser melting, *J. Alloys Compd.* 513 (2012) 518–523.
- [12] A.A. Popovich, V.Sh. Sufiiarov, I.A. Polozov, E.V. Borisov, Microstructure and mechanical properties of Inconel 718 produced by SLM and subsequent heat treatment, *Key Eng. Mater.* 651–653 (2015) 665–670.
- [13] I. Yadroitsev, I. Shishkovsky, P. Bertrand, I. Smurov, Manufacturing of fine-structured 3D porous filter elements by selective laser melting, *Appl. Surf. Sci.* 255 (2009) 5523–5527.
- [14] K. Mumtaz, N. Hopkinson, Selective laser melting of thin wall parts using pulse shaping, *J. Mater. Process. Technol.* 210 (2010) 279–287.
- [15] B. Song, S. Dong, P. Coddet, H. Liao, C. Coddet, Fabrication of NiCr alloy parts by selective laser melting: columnar microstructure and anisotropic mechanical behaviour, *Mater. Des.* 53 (2010) 1–7.
- [16] T. Niendorf, S. Leuders, A. Riemer, H.A. Richard, T. Tröster, D. Schwarze, Highly anisotropic steel processed by selective laser melting, *Metall. Mater. Trans. B* 44 (2013) 794–796.
- [17] F. Geiger, K. Kunze, T. Etter, Tailoring the texture of IN738LC processed by selective laser melting (SLM) by specific scanning strategies, *Mater. Sci. Eng.* 661 (2016) 240–246.
- [18] V.A. Popovich, E.V. Borisov, A.A. Popovich, V.Sh. Sufiiarov, D.V. Masaylo, L. Alzine, Functionally graded Inconel 718 processed by additive manufacturing: crystallographic texture, anisotropy of microstructure and mechanical properties, *Mater. Des.* 114 (2016) 441–449.
- [19] AMS5664E Nickel Alloy, Corrosion and Heat Resistant, Bars, Forgings, and Rings 52.5Ni - 19Cr - 3.0Mo - 5.1Cb - 0.90Ti - 0.50Al - 18Fe Consumable Electrode or Vacuum Induction Melted 1950 °F (1066 °C) Solution Heat Treated, Precipitation Hardenable, (2006).
- [20] ISO 6892-2:2011, *Metallic Materials – Tensile Testing – Part 2: Method of Test at Elevated Temperature*, (2011).
- [21] V.A. Popovich, W. Geertsma, M. Janssen, I.M. Richardson, I.J. Bennett, Mechanical strength of silicon solar wafers characterized by ring-on-ring fracture strength test in combination with digital image correction, *EPD Congress*, John Wiley & Sons, Inc., 2015, pp. 241–248.
- [22] B. Radhakrishnan, R.G. Thorapson, Solidification of the nickel-base superalloy 718: a phase diagram approach, *Metall. Trans. A* 20A (1989) 2866–2868.
- [23] W. Tayon, R. Shenoy, M. Redding, K. Bird, R. Hafley, Correlation between microstructure and mechanical properties in an INCONEL 718 deposit produced via electron beam freeform fabrication, *J. Manuf. Sci. Eng.* 136 (2014).
- [24] J.J. Schirra, Effect of heat treatment variations on the hardness and mechanical properties of wrought Inconel 718, *Superalloys 718, 625, 706 and Various Derivatives*, 1997, pp. 431–438.
- [25] J.T. Guo, *Materials Science and Engineering for Superalloys*, Science Press, Beijing, 2008, pp. 353–360.
- [26] D. Clark, M.R. Bache, M.T. Whittaker, Microstructural characterization of a polycrystalline nickel-based superalloy processed via tungsten-intert-gas-shaped metal deposition, *Metall. Mater. Trans. B Process Metall. Mater. Process. Sci.* 418 (6) (2010) 1346–1353.
- [27] M. Segersäll, Nickel-based Single-Crystal Superalloys - The Crystal Orientation Influence on High Temperature Properties, PhD thesis Linköping University, 2013.
- [28] W.J. Sames, *Additive Manufacturing of Inconel 718 Using Electron Beam Melting: Processing, Post-processing and Mechanical Properties*, PhD dissertation Texas A & M University, 2015.
- [29] S.C. Lee, S.H. Chang, T.P. Tang, H.H. Ho, J.K. Chen, Improvement in the microstructure and tensile properties of Inconel 718 superalloy by HIP treatment, *Mater. Trans.* 47 (11) (2006) 2877–2881.
- [30] M. Schwartz, D. Gheorghe, R. Ciocoiu, I. Ciuca, G. Jula, Failure of an Inconel 718 die used in production of hot copper direct extrusion, *Mater. Sci. Eng.* 4 (6) (2015).
- [31] G. Sjöberg, N.G. Ingesten, R.G. Carlson, Grain boundary delta phase morphologies, carbides and notch rupture sensitivity of cast alloy 718, *Miner. Met. Mater. Soc.* (1991) 603–620.
- [32] B. Baufeld, Mechanical properties of INCONEL 718 parts manufactured by shaped metal deposition (SMD), *J. Mater. Eng. Perform.* 21 (7) (2012) 1416–1421.
- [33] W. D. Callister, *Fundamentals of Materials Science and Engineering*, 2nd ed. Wiley & Sons, pp. 252.
- [34] T. Trosch, J. Ströföner, R. Völkl, U. Glatzel, Microstructure and mechanical properties of selective laser melted Inconel 718 compared to forging and casting, *Mater. Lett.* 164 (2016) 428–431.
- [35] R.W. Hertzberg, *Deformation and Fracture Mechanics of Engineering Materials*, John Wiley & Sons Inc (1996).
- [36] Y.N. Zhang, X. Cao, P. Wanjara, M. Medraj, Oxide films in laser additive manufactured Inconel 718, *Acta Mater.* 61 (2013) 6562–6576.
- [37] A.K.M.B. Rashid, J. Campbell, Oxide defects in a vacuum investment-cast Ni-based turbine blade, *Metall. Mater. Trans. A* 35A (2004) 2063–2071.
- [38] J. Campbell, M. Tiryakioglu, Bifilm defects in Ni-based alloy castings, *Metall. Mater. Trans. A* 43B (2012) 902–914.